

Article

Experimental Study of Thermal and Pressure Performance of Porous Heat Sink Subjected to Al₂O₃-H₂O Nanofluid

Oguzhan OZBALCI ^{1,*}, Ayla DOGAN ¹ and Meltem ASILTURK ²¹ Department of Mechanical Engineering, Akdeniz University, Antalya 07058, Turkey² Department of Material Science and Engineering, Akdeniz University, Antalya 07058, Turkey

* Correspondence: oguzhanozbalci@gmail.com

Abstract: With the developing technology, the dimensions of electronic systems are becoming smaller, and their performance and the amount of energy they need increases. This situation causes the electronic components to heat up more and the existing cooling systems to become inadequate. In this study, instead of the fins used in existing systems, 10 PPI and 40 PPI PHS were placed inside a water block, and the Al₂O₃-H₂O nanofluid at a mass fraction of 0.1% was used as the cooling fluid. Experiments were carried out under constant heat flux of 454.54 W/m² and 1818.18 W/m², with volumetric flow rates varying between 100 mL/min and 800 mL/min. The heat transfer results were compared with the results obtained from the base fluid and the empty surface. The results showed that the nanofluid reduced the surface temperatures compared to the base fluid. Especially when PHSs were used together with the nanofluid, a significant increase in heat transfer occurred compared to the empty surface. The highest heat transfer was observed when both the nanofluid and 40 PPI PHS were used together. In addition, the highest thermal performance value was determined as 1.25 times compared to the empty surface when the nanofluid and 10 PPI PHS were used together.

Keywords: electronic cooling; nanofluids; water block; metal foam heat sink



Citation: OZBALCI, O.; DOGAN, A.; ASILTURK, M. Experimental Study of Thermal and Pressure Performance of Porous Heat Sink Subjected to Al₂O₃-H₂O Nanofluid. *Electronics* **2022**, *11*, 2471. <https://doi.org/10.3390/electronics11152471>

Academic Editors: Ciro Aprea, Adrián Mota Babiloni, Juan Manuel Belman-Flores, Rodrigo Llopis, Angelo Maiorino, Jaka Tušek and Andrej Žerovnik

Received: 11 July 2022

Accepted: 4 August 2022

Published: 8 August 2022

Publisher's Note: MDPI stays neutral with regard to jurisdictional claims in published maps and institutional affiliations.



Copyright: © 2022 by the authors. Licensee MDPI, Basel, Switzerland. This article is an open access article distributed under the terms and conditions of the Creative Commons Attribution (CC BY) license (<https://creativecommons.org/licenses/by/4.0/>).

1. Introduction

Electronic elements working with electrical energy accumulate their excess energy as heat energy in their structure. This heat must be removed from the element with appropriate cooling methods. Otherwise, temperature increase may occur on the element, its performance may decrease, and then, it may be damaged and become unusable. With the developing technology, the dimensions of electronic systems are becoming smaller and smaller. Since this situation causes more heat production per unit area, it results in the cooling systems currently in use being insufficient. Research works are generally aimed at increasing the contact surface area (finned surfaces) and improving the coolant used. As is known, finned structures made of different materials (aluminum, copper, etc.) are used to expand the surface area in the cooling of electronic systems. Either water or air is commonly used as the cooling fluid. One of the most important features of water cooling over air cooling is that the thermal conductivity of water is 25 times higher than that of air. In this way, water can transfer heat from the area where the fan is located much faster than air. Since liquid cooling removes heat faster than air, it enables the processor to run at higher speeds. To provide more effective cooling, researchers have started to work on producing new types of fluids with higher cooling capacity by adding materials with high thermal conductivity to a fluid chosen as the base fluid.

In the literature, many finned heat sinks of different shapes and sizes were used in the studies to provide effective cooling in the heated areas. PHSs with high surface area/volume ratios are also materials that are currently being researched in this context. Similarly, there are many studies in the literature on the development of the cooling fluid used in electronic systems.

The use of nanofluids in the cooling of electronic systems is one of the most researched topics today. The nanofluids prepared by adding nanoparticles with certain concentrations into the base fluid were first studied by Choi and Eastman [1]. They obtained a new fluid by mixing materials with high thermal conductivity into the base fluid at certain concentrations (volumetric or mass) and named this fluid a nanofluid.

Pourfarzad et al. [2] experimentally investigated the effect of using alumina-water nanofluids with volumetric concentrations of 0.1%, 0.3% and 0.5% on heat transfer and pressure drop in a miniature heat sink with a porous structure. Heat sinks made of copper material with two different pore densities, 15 PPI and 30 PPI, were placed in the channel. From the results, the amount of improvement in the heat transfer coefficient obtained for 15 PPI and 30 PPI with the use of nanofluids at different volumetric concentrations varied between 1 and 22%, and 2 and 26.4%, respectively.

Bayomy et al. [3–6] carried out many experimental and numerical studies using the same experimental setup to investigate the use of metal foam cooler in electronic cooling. Firstly, they investigated the use of a metal foam heat sink with pure water to cool the Intel core i7 processor. Then, they investigated the use of metal foam heat sink and nanofluid in the same setup. In their last two studies, they investigated the effect of metal foam heat sinks with different numbers of channels in them and metal foam heat sinks with different numbers of aluminum fins inside on heat transfer. In the results obtained, it was determined that the use of metal foam heat sink improved the heat transfer by 20% compared to the empty channel. When the Reynolds number was 601.3 and 210, using 0.2% Al_2O_3 nanofluid by volume, an improvement of 37% and 28%, respectively, of the average Nusselt number compared to pure water was obtained. Compared to metal foams with a different number of channels, lower local temperatures were obtained in the finless metal foam heat sink. In the metal foam heat sink with four aluminum fins, higher local Nusselt numbers were obtained compared to the metal foam heat sink with three and five fins.

The cooling effects of nanofluid passing through copper foam heat sinks with different pore densities (20, 30 and 40 PPI) were investigated by Qi et al. [7]. Experiments were carried out for the Reynolds number ranging from 414 to 1119. The TiO_2 -water nanofluid with the mass concentration between 0.1% and 0.5% was used as the coolant. When the results were examined, the lowest surface temperatures were obtained with the use of 0.3 wt% TiO_2 -water nanofluid compared to pure water, and as a result, a 35.7% improvement in heat transfer was observed.

Boomsma et al. [8] investigated the thermal performance of open-cell aluminum foam (6101–T6 alloy) heat exchanger under forced convection conditions. Water was used as the cooling fluid. Open-cell aluminum foam materials were compressed and formed into heat exchangers for electronic cooling applications that dissipate large amounts heat. In the study, it was determined that compressed aluminum metal foams had a significant effect on both the improvement of heat transfer and efficiency compared to the commercially used heat exchangers. It was determined that the pumping power required for the compressed open-cell aluminum foam heat exchangers used in the study was the same, but they showed 2–3 times lower thermal resistance than the commercial heat exchangers.

Saghir and Welsford [9] presented a numerical assessment of the use of TiO_2 and Al_2O_3 nanofluids working with ethylene glycol and water as the base fluid inside porous media. In addition, an experimental evaluation of Al_2O_3 -water nanofluids was made. When the numerical analysis and experimental results were compared, the deviation in temperature value was found to be less than two degrees. When all the numerically obtained results were compared, it was determined that ethylene glycol provided the highest average Nusselt number, while water required significantly lower pumping power.

Delisle et al. [10] investigated the effect of using the Al_2O_3 -water nanofluid in a plate-finned heat sink filled with 10 PPI and 20 PPI aluminum foam material in their study on heat transfer, experimentally and numerically. The Al_2O_3 -water nanofluid with a concentration of 0.6% by volume was used as the cooling fluid. From the results, when a 20 PPI triple-

finned heat sink and Al_2O_3 -water nanofluid with 0.6% concentration by volume were used, the highest value of the average Nusselt number was obtained as 135.5.

Ameri et al. [11] numerically investigated the effect of using nanofluids on heat transfer in a pipe filled with metal foam. Experiments were carried out for the Reynolds number varying from 200 to 1000. The Fe_3O_4 -water nanofluid with an average concentration of 0.5% to 2% was used as the cooling fluid. The porosity of the metal foam material used in the measurements varied between 0.7 and 0.9. From the results, it was determined that the Nusselt number varied directly with the mean concentration and the Reynolds number, but it varied inversely with porosity.

Nazari et al. [12] experimentally investigated the effect of heat transfer by passing the Al_2O_3 -water nanofluid through a pipe filled with metal foam under forced convection conditions. The Al_2O_3 -water nanofluid with volumetric concentrations of 0.1%, 0.25%, 0.5%, 1% and 1.5% was used as a refrigerant, and the obtained results were compared with pure water and empty pipe. The results showed that increasing the alumina nanofluid concentration augmented the amount of heat transfer. Compared to the empty tube, the maximum enhancement in the Nusselt number was found to be approximately 57% for a volumetric concentration of 1.5% Al_2O_3 nanofluid inside the tube filled with metal foam at $\text{Re} = 3704$.

An experimental investigation of the effect of using an MgO nanofluid in a copper pipe, which was partially filled with 70% porosity metal foam, was presented by Rabbani et al. [13]. From the inner surface of the copper pipe, 1 cm in the first sample and 1.8 cm in the second sample were covered with metal foam material. The MgO nanofluid with volumetric concentrations of 0.5%, 0.25% and 0.0625% was used as a cooling fluid. Compared to the base fluid, with the use of nanofluid for the first and the second samples, the average convection heat transfer coefficient was increased by about 9% and 15%, respectively.

Aliabadi and Hormozi [14] conducted an experimental study to investigate the effects of simultaneous use of a pin channel and CuO-water nanofluid on the performance of plate-fin heat exchangers. Experimental results were compared with the empty channel; the pinned channel considerably increased the thermal-hydraulic performance of the plate-fin heat exchanger, by about 38%. Although there was a significant improvement in the heat transfer coefficient compared to the base fluid with the use of nanofluid, it was determined that there was an increase in the pressure drop.

The variation in the thermal and hydraulic performance of a tangential miniature heat sink using the Al_2O_3 -water and TiO_2 -water nanofluids was experimentally determined by Miry et al. [15]. Studies were carried out at the same volumetric concentrations (0.5%, 1%, 1.5% and 2%) for both fluids. With the use of Al_2O_3 -water and TiO_2 -water compared to pure water, it was observed that the average temperature of the heat sink decreased by 2.2 °C and 1.6 °C, respectively. In addition, the convection heat transfer coefficient obtained from the Al_2O_3 -water and TiO_2 -water nanofluids increased by 15% and 12%, respectively, compared to water at the Reynolds numbers in the range of 210–1100.

The effect of 10 PPI, 20 PPI and 40 PPI aluminum metal foam heat sinks placed in a 3×3 arrangement in a partially open cavity on natural and forced convection heat transfer was experimentally investigated [16,17]. In both studies, the most heated elements were determined, and solutions were offered for the appropriate cooling process. The natural convection heat transfer in an inclined rectangular duct with metal foam heat sinks placed separately on its surface was investigated experimentally by Dogan and Ozbalci [18].

The effect of using a copper-foam-filled copper tube and an R245fa refrigerant on heat transfer and pressure drop was experimentally investigated by Abadi and Kim [19]. The obtained data were compared with correlations in the literature. New correlations were proposed for the heat transfer and pressure drop of small tubes filled with the foam material.

The effect of 5 and 20 PPI metal foam heat sinks with one, two, four and six fins on forced convection heat transfer was investigated by Bhattacharya and Mahajan [20]. According to the results obtained, it was observed that the heat transfer increased when

the fins were used with metal foam heat sinks. They stated that the heat transfer coefficient increased with the increase in the number of fins, but after a certain number of fins, the heat transfer was decreased depending on the interfacial boundary layer. It was determined that the optimum geometry was the use of four fins in a 20 PPI sample. Experiments were performed with one, two and four fin samples on a 5 PPI metal foam heat sink, and similar results were obtained with a 20 PPI heat sink.

The effects of 10 PPI and 20 PPI metal foam heat sinks and pin-finned metal foam heat sinks with the same pore density on heat transfer in electronic cooling were experimentally and numerically investigated [21,22].

The effects of using water blocks with different shapes and sizes of heat sink surfaces together with nanofluids in heat transfer were investigated in many studies [23–30]. In the studies, the nanofluids prepared with different concentrations and different nanoparticles were compared with the base fluid. The obtained results from all studies showed that the heat transfer was increased significantly with the use of nanofluids in the water block.

The effect of nanofluids prepared by adding CeO_2 , Al_2O_3 and ZrO_2 nanoparticles at concentrations ranging from 0.5% to 2% into a mixture of 20% ethylene glycol and 80% distilled water on the cooling performance in a microchannel heat sink was investigated by Alfaryjat et al. [31]. The highest increase in heat transfer coefficient was obtained with the CeO_2 nanofluid, with 29%. In addition, an increase of 22% and 17% was observed with the use of Al_2O_3 and ZrO_2 nanofluids, respectively.

Ali and Arshad [32,33] investigated the effect of using different nanofluids on heat transfer in the mini-channel where square-section pin fins prepared in different arrays and angles are used. In the first study, $\text{TiO}_2(\text{Anatase})/\text{H}_2\text{O}$ and $\text{TiO}_2(\text{Rutile})/\text{H}_2\text{O}$ nanofluids prepared at 4.31% and 3.99% volume concentrations by volume were used. When the results were examined, more heat transfer amount was obtained in the same fluid in the staggered pin fin heat sink than in the inline pin fin heat sink. For both geometries, $\text{TiO}_2(\text{Rutile})/\text{H}_2\text{O}$ nanofluids showed better thermal performance than $\text{TiO}_2(\text{Anatase})/\text{H}_2\text{O}$ nanofluids. In the second study, experiments were carried out in three different heat sinks with channel angles of 22.5, 45 and 90 degrees using water-based graphene nanoplatelets (GNPs) nanofluid with a concentration of 9.5% by volume. According to the results, the thermal performance values of the heat sink with a channel angle of 22.5 degrees were better than the other heat sinks.

The effect of using nanofluids with heat sinks prepared in different chevron fin shapes on heat transfer was investigated experimentally and numerically by Hassani et al. [34]. In the experiments, water and different volumetric concentrations (0.5% and 1%) of the Al_2O_3 -water nanofluid were used together with the heat sink in seven different shapes. According to the results, a high rate of heat transfer was achieved due to the decrease in the surface temperature of the chevron shape finned heat sinks and the increase outlet temperature of the coolant.

The effects of using nanofluids in mini-channels with different shapes and sizes [35–37] and small-diameter tubes [38,39] on heat transfer were also investigated. It was found that the surface temperatures of both mini-channels and small-diameter tubes decrease with the use of nanofluids of different concentrations. In addition, it was stated that the surface temperatures were also affected by the shape and dimensions of the mini-channel. In studies with wavy mini-channel heat sinks, it was determined that the Nusselt number was more affected by the wavelength than the channel width.

Experimental analysis of the use of offset strip miniature heat sinks prepared in different strip shapes and thicknesses with the Al_2O_3 -water nanofluid was conducted by Aliabadi et al. [40]. From the results, better cooling performance was obtained with the use of miniature heat sinks with the nanofluid than with the use of the base fluid.

The effect of particle size on heat transfer with the use of the Al_2O_3 -water nanofluid in a tube was investigated by Anoop et al. [41]. Two different particle sizes of alumina-water nanofluid were prepared. From the results, it was determined that a higher heat transfer was achieved with the use of the nanofluid than the base fluid, and the highest convection

heat transfer coefficient values were obtained with nanofluid with a particle size of 45 nm. When x/D was 145, the Reynolds number was 1550, and the nanofluid was used at 4% concentration by mass, an approximately 25% increase in heat transfer coefficient with the use of nanofluids with 45 nm particle size and an 11% increase with the use of nanofluids with 150 nm particle size were determined.

The effects of using pin fin heat sinks and nanofluids prepared in different ways on heat transfer and pressure drop were experimentally investigated by Duangthongsuk and Wongwises [42]. Experiments were carried out with the Reynolds number ranging from 700 to 3700 and heat flux values of 2 and 5 W/cm². It was stated that the heat transfer increased with the increase in the Reynolds number and particle size.

The effect of the use of the Al₂O₃ nanofluid on the cooling performance in a mini-channel heat sink was experimentally investigated by Ghasemi and Hosseini [43]. It was determined that the use of the nanofluid showed much better thermal performance and higher average heat transfer coefficient than the base fluid. Apart from that, there was a slight increase in the pumping power with the use of the nanofluid.

The mathematical model of peristaltic flow of the Rabinowitsch fluid in a rectangular duct was designed by Nadeem et al. [44]. Physical parameters were used to determine the velocity distribution, pressure gradient, pressure rise, convection and entropy values for both the dilatant and pseudo-plastic fluids. It was determined that the dilatant nature of the fluid had higher convection rates compared to the pseudo-plastic fluid.

The peristaltic flow of single-walled and multi-walled carbon nanotube water-based nanofluids in a wavy rectangular channel was analyzed by Nadeem et al. [45] using the Eigenfunction expansion method. From the results, it was determined that the single-walled carbon nanotube/water nanofluid has a higher temperature profile than the hybrid nanofluid (single-walled + multi-walled carbon nanotube/water). It was seen that nanofluids have an important role in the improvement of thermal conductivity.

A mathematical model of the peristaltic flow of multi-walled carbon nanotubes in an elliptical channel with ciliated walls was designed by Ghazwani et al. [46]. According to the results obtained, it was determined that the thermal conductivity of the fluid increased, and the base fluid temperature decreased with the increase in carbon nanotube concentration. The combined mathematical analysis of heat and mass transfer of peristaltic flow in an elliptical vertical duct was investigated by Nadeem et al. [47]. When the results were examined, it was determined that the concentration profile had a parabolic shape and an axially symmetrical behavior.

As a result of the detailed literature research, it was determined that the experimental studies on the use of PHS and nanofluids in the cooling of electronic systems were limited. Therefore, it was seen that there was a need for extensive research on the thermal behavior and pressure drop of aluminum PHSs with different pore densities exposed to nanofluid, especially for the cooling of electronic elements. In this paper, the effects of using 10 PPI and 40 PPI PHSs with nanofluid on the thermal and pressure performance of CPU cooling systems were experimentally investigated. Al₂O₃-water nanofluid with a concentration of 0.1% by mass was used as the cooling fluid. The results obtained by using the nanofluid with 10 PPI and 40 PPI PHSs were compared with pure water and empty channel. By comparing the use of promising PHSs and nanofluids separately and together in electronic cooling, it was investigated in which case more effective cooling was achieved. Apart from this, the effect of pore density on cooling was investigated in detail with the use of 10 PPI and 40 PPI PHSs, with both the basic fluid and the nanofluid.

2. Material and Method

2.1. Experimental Setup

Nanofluids are innovative materials that are still being investigated for use in many different areas (solar collectors, automobile radiators, electronic devices, etc.) due to their higher thermal conductivity coefficients in cooling applications compared to commercial fluids. In addition, it is noteworthy that PHSs are preferred, especially in electronic cooling

applications due to their high thermal performance. In the present study, the appearance of the experimental setup to examine the effect of using these two promising materials together on heat transfer and pressure drop for electronic cooling systems is given in Figure 1.

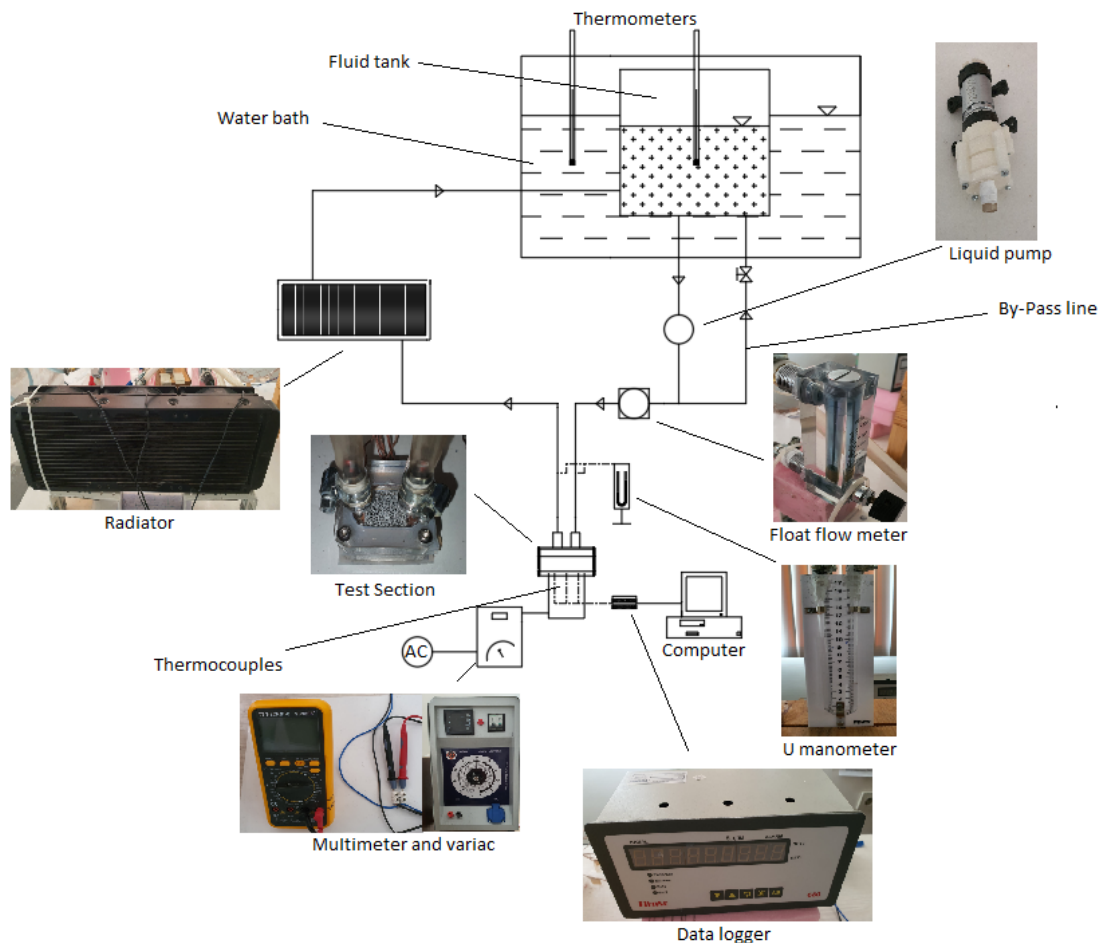


Figure 1. Schematic diagram of experimental setup.

The experimental setup operated in a closed loop consisted of a pump, by-pass line, test area, radiator and liquid tank. The volumetric flow rate of the fluids ranged from 100 mL/min to 800 mL/min, and a 12 V liquid pump was used for fluid circulation. Thirty-gauge copper-constantan thermocouples and thermometers were used for temperature measurements. Signals from the thermocouples were collected, processed, stored and analyzed using the ELIMKO brand data acquisition system. A total of 9 thermocouples were used in the test area. Three of these were placed at the bottom of the water block, two of these were placed at the entrance and exit section of the fluid, and four of these were placed symmetrically on the bottom and top of the insulation material. The amount of pressure drop between the inlet and outlet sections of the test area was measured with a U manometer.

In the study, a 5×5 cm electric heater with 88Ω resistance was used to represent the heated electronic elements (CPU). The voltage of the electric current applied to the heater was controlled by means of a TT Technic VC-9808+ multimeter and variac. A constant temperature water bath was used to keep the temperature of the fluid entering the test area as constant as possible and for it not to be affected by changes in room temperature during the day. The liquid tank used for the storage of the fluid in the study was placed in a constant temperature water bath, and the temperature of the two tanks was controlled with thermometers.

In the cooling of electronic systems, a commercial water block was used as the test area, and the experiments were carried out by placing aluminum Al-6101 alloy PHSs with different pore densities (10 PPI and 40 PPI) inside. The bottom part of the water block was made of a copper plate, and the other sides were made of plexiglass. The characteristics of the porous heat sinks are given in Table 1, and their appearance is given in Figure 2. In order to ensure full contact with the copper plate, the base of the PHSs was manufactured as a very thin aluminum plate with a thickness of 1 mm. A thermal pad with high thermal conductivity (ARTIC brand thermal pad, 0.5 mm, 6 W/mK) was used to reduce the contact resistance by ensuring the adhesion of aluminum PHSs and copper surface as much as possible.

Table 1. Aluminum (Al 6061) PHSs properties.

Pore Density (PPI)	10 (Al-6101)	40 (Al-6101)
Porosity (ϵ)	0.910	0.910
Permeability (m^2)	7.73×10^{-8}	2.40×10^{-8}
Thermal conductivity (W/mK) (Kati)	218	218
Dimensions (m) ($\times 10^{-3}$)	$25 \times 25 \times 10$	$25 \times 25 \times 10$

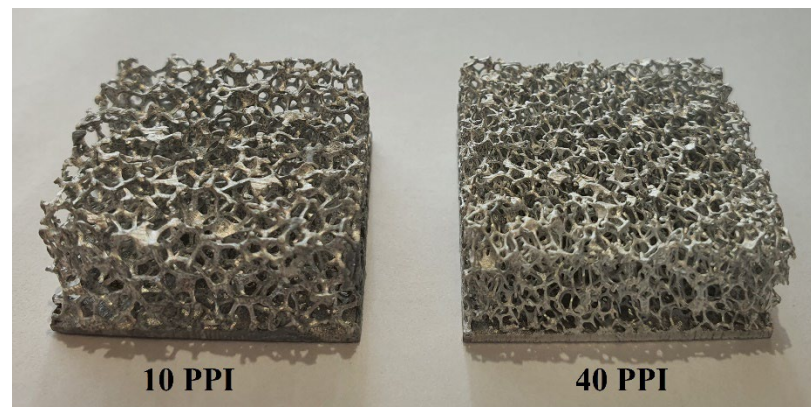


Figure 2. Appearance of aluminum PHSs with the pore density of 10 PPI and 40 PPI.

The schematic drawing of the test area is given in Figure 3. Since the heat losses from the side and top of the water block were very small, they were neglected. Glass wool and foamboard with dimensions of $5 \times 5 \times 5 \text{ cm}^3$ were placed under the test area in order to reduce the heat losses that may occur only from the lower part of the water block. As a result of the calculations, it was determined that the transmission losses were 0.55% of the total power supplied by the electric heater. The radiation losses were neglected. It was observed that steady-state conditions were reached after approximately 1.5 h for each experiment.

2.2. Preparations of Nanofluids

In this study, ultrapure water, as the basic fluid, and Al_2O_3 nanoparticles with the trade name Aeroxide Alu130 (Evonik Ind. AG, Essen, Germany) were used to prepare the nanofluid. The appearance of both the base fluid and the nanofluid used in the study are given in Figure 4a. The density and surface area of Al_2O_3 nanoparticles were 3.27 g/cm^3 and $130 \pm 20 \text{ m}^2/\text{g}$, respectively. The shape and size of the Al_2O_3 nanoparticles were examined with the FEI transmission electron microscope, which was set to 120 kV accelerating voltage. For the analysis, Al_2O_3 - H_2O dispersion was dropped on the carbon-coated copper grid and was dried. Particle size distribution and mean particle size of Al_2O_3 nanoparticles were determined from TEM images using the Image J program. As seen in Figure 4b, the particles have a spherical shape and a monomodal distribution. The mean

particle size of the Al_2O_3 nanoparticles is 9.21 ± 0.56 nm. The properties of the Al_2O_3 nanoparticles are given in Table 2.

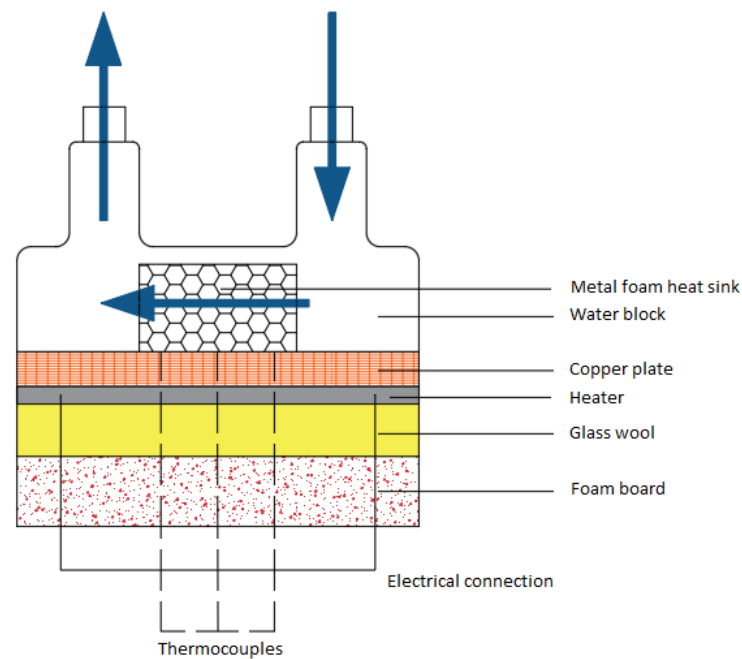


Figure 3. Test section's detailed schematic drawing.

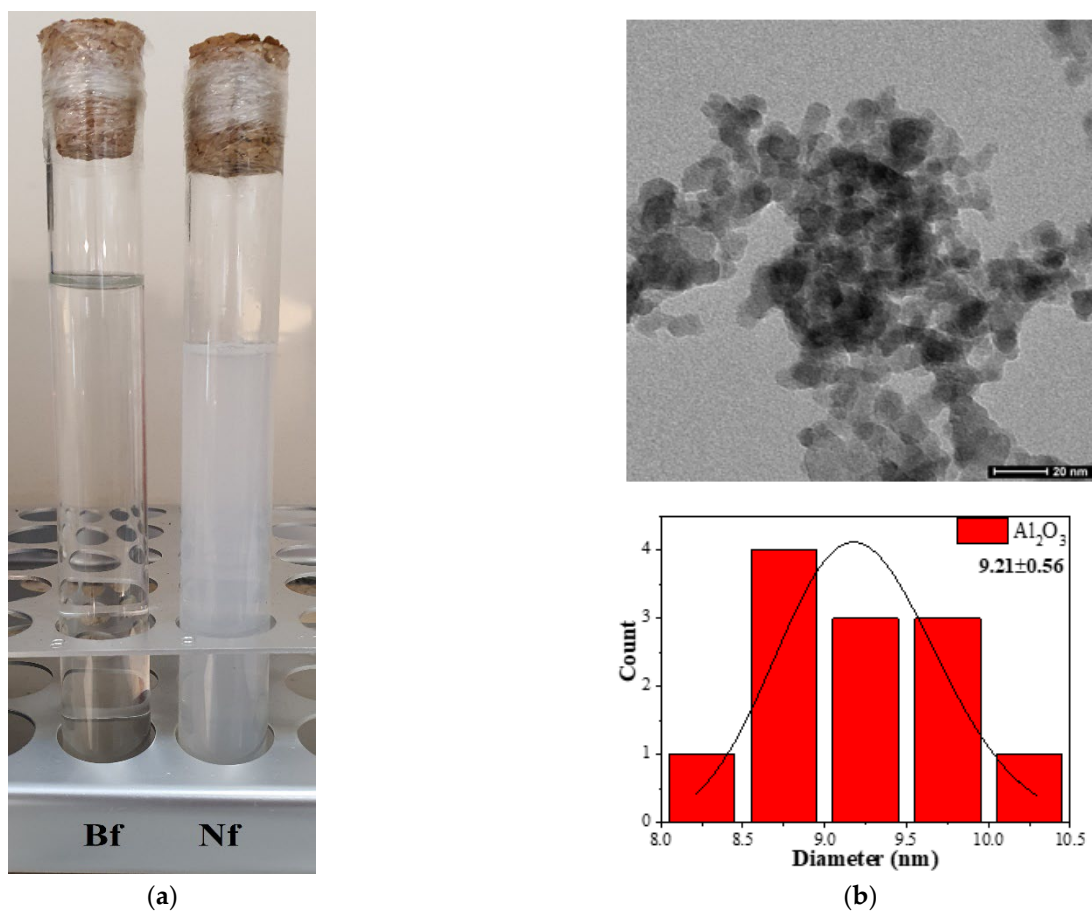


Figure 4. (a) Appearance of base fluid (deionized water) and fraction of 0.1% Al_2O_3 - H_2O nanofluid by mass; (b) TEM image and particles size distribution graph of Al_2O_3 nanoparticles.

Table 2. The properties of Al₂O₃ nanoparticles, which were used for nanofluid preparation [48].

Specific Surface Area	130 ± 20 m ² /g
Tamped Density	50 g/L
PH (in %4 dispersion)	4.4–5.4
Density	3.27 g/cm ³

While preparing the nanofluid with a concentration of 0.1% (*w/w*), the desired amount of nanoparticles was mixed with ultrapure water, and then, ultrasonic treatment (Elma, Elmasonic S100 H, 50 Hz, Elma Schmidbauer GmbH, Singen, Germany) was applied for 2 h. A stable and transparent colloid was obtained in which no precipitation was observed throughout the entire experimental study. The density of the prepared nanofluid was measured with a 25 mL volume pycnometer, and its viscosity was measured with the Fungi Lab ALPL model viscometer. The heat capacity [49] and thermal conductivity coefficient [50] of the nanofluid were taken from the literature. The thermophysical properties of the nanofluid at the specified concentration are presented in Table 3.

Table 3. Base fluid and nanofluid thermophysical properties.

Fluid	Density (ρ) (g/cm ³)	Viscosity (μ) (kg/ms)	Thermal Conductivity (k) (W/mK)	Specific Heat (C_p) (kJ/kgK)
Water	0.9984	0.00098	0.5962	4182.8
(<i>w/w</i>) 0.1% Al ₂ O ₃ -Water	0.9986	0.00134	0.5973	4181.8

In the studies with nanofluid, both mass and volumetric concentration values were used. The relationship between mass concentration and volumetric concentration was determined by the following equation [27].

$$\varphi = \frac{1}{(1/\omega)(\rho_p/\rho_{nf})} \quad (1)$$

In this equation, φ was the volumetric concentration, ω was the mass concentration, ρ_p was the density of the nanoparticle, and ρ_{nf} was the density of the nanofluid.

The specific heat of the nanofluid was determined according to the following equation [27].

$$C_{p_{nf}} = \varphi C_{p_{np}} + (1 - \varphi) C_{p_{bf}} \quad (2)$$

here, $C_{p_{nf}}$, $C_{p_{np}}$ and $C_{p_{bf}}$ were the specific heat of the nanofluid, nanoparticle and base fluid, respectively.

2.3. Calculation of Experimental Data

The amount of heat transferred from the heated surface to the fluid in the test section was calculated from the energy balance and is expressed below.

$$\dot{Q}_{Conv.} = \dot{Q}_{Heater} - \dot{Q}_{Cond.} \quad (3)$$

here, \dot{Q}_{Heater} represents the total amount of heat taken from the electric heater, and $\dot{Q}_{Cond.}$ represents the heat losses by conduction from the bottom of the test section. In this calculation, the total heat addition from the electrical heater and conduction losses at the bottom of test section were determined as shown below.

$$\dot{Q}_{Heater} = \frac{V^2}{R} \quad (4)$$

$$\dot{Q}_{Cond.} = -kA_s \frac{\Delta T}{\Delta x} \quad (5)$$

In Equation (4), V and R were the electrical voltage and resistance applied to the heater, respectively. The thermal conductivity coefficient of the insulation foam was k , the surface area was A_s , the temperature difference between the two surfaces of the insulation material was ΔT , and the thickness of the insulation material was Δx in Equation (5). The amount of heat transferred from the heated surface to the fluid per unit area was calculated as follows.

$$q_{conv.} = \frac{\dot{Q}_{conv.}}{A_s} \quad (6)$$

The inlet temperature of the fluid was taken into account in determining the mean surface temperature of the test section.

$$T^*_{Smean} = T_{Smean} - T_i \quad (7)$$

In the test section, the mean surface temperature was represented by T^*_{Smean} , and the fluid inlet temperature was represented by T_i . The mean arithmetic temperature of the surface was represented T_{Smean} and calculated from

$$T_{Smean} = \frac{(T_1 + T_2 + T_3)}{3} \quad (8)$$

The mean convection heat transfer coefficient (h) and the mean Nusselt number (Nu) were calculated using the following equation.

$$h_{mean} = \frac{q_{conv.}}{T_{Smean} - T_i} \quad (9)$$

$$Nu_{mean} = \frac{h_{mean} D_h}{k_f} \quad (10)$$

here, h_{mean} , Nu_{mean} were the mean convection heat transfer coefficient and the mean Nusselt number, respectively. The mean Nusselt number was calculated according to the hydraulic diameter (D_h). The hydraulic diameter is given below.

$$D_h = \frac{4A_c}{P} \quad (11)$$

where A_c was the cross-sectional area, and P was the perimeter of the channel.

The thermal resistance between the surface and the fluid in the test region was calculated using the equation below.

$$R_{th} = \frac{T_{Smean} - T_i}{\dot{Q}_{Conv.}} \quad (12)$$

The thermal performance of the nanofluid relative to the base fluid can be measured using the heat transfer efficiency (ε_h) equation [51].

$$\varepsilon_h = \frac{h_{nf}}{h_{bf}} \quad (13)$$

Pumping power, taking into account the increase in the pressure drop calculated from

$$P_p = \dot{V} \Delta P \quad (14)$$

where \dot{V} and ΔP represent the volumetric flow rate and the pressure difference, respectively. The thermal performance index was used to compare the changes in thermal and hydraulic

performance as a result of the use of the nanofluid with PHS and was calculated with the following formula [2].

$$\eta = \frac{\frac{Nu_{mean,nf,foam}}{Nu_{mean,nf,empty}}}{\frac{\Delta P_{nf,foam}}{\Delta P_{nf,empty}}} \quad (15)$$

2.4. Uncertainty Analysis

Uncertainty analysis was conducted to ensure the accuracy and reliability of the results obtained from the experimental study. Within this scope, the uncertainty analysis was performed using the current sensitivity ratios of each measuring equipment given in Table 4. The uncertainty analysis [52] was calculated using the following equation.

$$w_f = \left[\left(\frac{\partial f}{\partial x} w_x \right)^2 + \left(\frac{\partial f}{\partial y} w_y \right)^2 + \dots \right]^{1/2} \quad (16)$$

Table 4. Measuring equipment properties and sensitivities.

Measurement Tools	Sensibility	Uncertainties
T-type Thermocouples	±1.5%	0.015%
TT Technic VC-9808+	±0.8% +5 (AC)	0.14%
TT Technic VC-9808+	±0.8% +3 (Ohm)	0.042%
Float Flowmeter	±3%	0.03%

In general, the uncertainties in the heat transfer coefficient, thermal resistance, heat transfer efficiency, pumping power and Nusselt number were calculated as 1.501%, 1.38%, 1.46%, 2.08% and 2.078%, respectively.

3. Results and Discussion

In the present study, the effects of the combined use of the nanofluid and PHS on heat transfer and pressure drop were investigated experimentally, and the Al₂O₃-H₂O nanofluid was used as the cooling fluid at a concentration of 0.1% (*w/w*) by mass. Experiments were carried out for all surfaces (empty, 10 PPI and 40 PPI) at 454.54 W/m² and 1818.18 W/m² constant heat flux and volume flow range from 100 mL/min to 800 mL/min. The results were compared with the heat transfer and pressure drop results obtained with the base fluid. In Figure 5, the change in the pressure drop for both the nanofluid and the base fluid according to the volumetric flow rate is given. When the nanofluid was used as a cooling fluid, an increase in pressure drop was observed for all surfaces. The increase in pressure drop with the use of the nanofluid compared to the base fluid increased further with the addition of PHSs. It was determined that the pressure drop in the heat sink with a pore density of 40 PPI is higher than that of the 10 PPI for both fluids. The larger the pore density, the greater the web connection intensity, resulting in increased flow resistance. There was no significant change in pressure drop for all conditions at low volumetric flow rates (≤200 mL/min). However, when nanofluid was used at flow rates greater than 200 mL/min, an increase in the pressure drop gradient from 7.29% to 17.94% was observed in the 40 PPI PHS compared to the 10 PPI PHS. In addition, in the case of using the base fluid, an increase in the pressure drop gradient from 20% to 27.50% was observed.

As a result of using both the nanofluid and PHS (10 PPI and 40 PPI), the variation of average surface temperatures according to volumetric flow at 1818.18 W/m² constant heat flux are given in Figure 6A,B. When both figures were examined together, with the use of the nanofluid, a significant decrease in the average surface temperature was observed on all surfaces compared to the base fluid. In the case of using a 10 PPI PHS, it was seen that the nanofluid lowered the surface temperature more than the base fluid (Figure 6A). In addition, when the data obtained from the 10 PPI PHS were compared with the empty surface, it was determined that the surface temperatures decreased significantly. While

the difference between the surface temperatures was more pronounced in all cases at low volumetric flow rates, the surface temperatures approached each other with the increase in the volumetric flow rate. Results from the use of 40 PPI PHS under the same conditions are given in Figure 6B. Compared to 10 PPI PHS, the surface temperatures of 40 PPI PHS were seen to be close to each other.

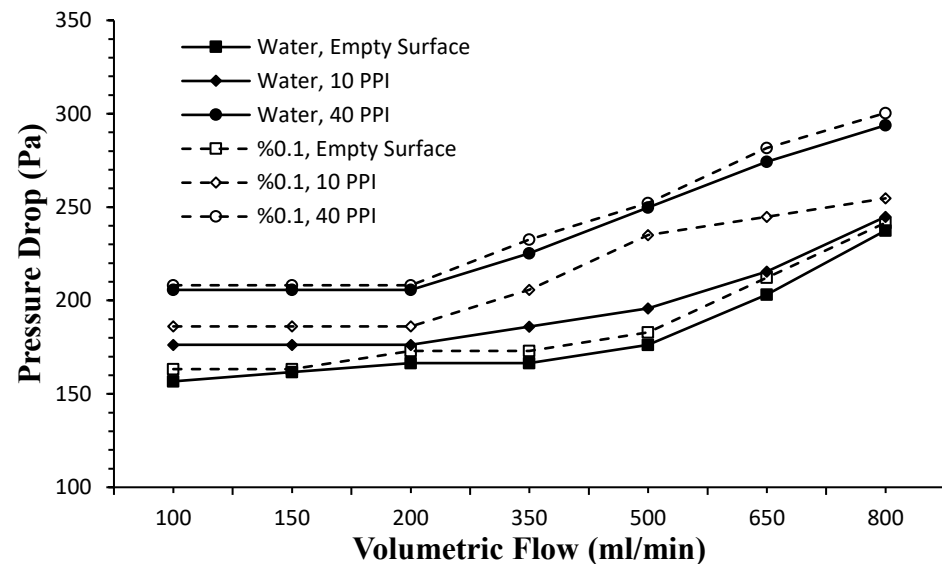


Figure 5. Effect of using nanofluid and porous HS on pressure drop.

At 1818.18 W/m^2 constant heat flux, the variation of the convective heat transfer coefficient and the Nusselt number according to the volumetric flow rate with the use of the nanofluid and PHSs are given in Figures 7 and 8. When both figures were examined together, it was observed that h_{mean} and Nu_{mean} were increased with the increase in volumetric flow rate with the use of the nanofluid on all surfaces compared to the base fluid. Results with the use of the nanofluid and the base fluid in 10 PPI and 40 PPI PHSs are given in figures separately. With the use of the nanofluid, higher h_{mean} and Nu_{mean} were obtained in the PHS compared to the base fluid. In addition, it was observed that h_{mean} and Nu_{mean} were increased for both fluids with the use of PHS compared to the empty surface. This is because two types of heat transfer mechanisms take place in the PHS. The first of these is that the metal foam materials with a high area/volume ratio greatly increase the thermal conductivity due to their skeleton structures, and the other is that they increase the convection heat transfer by mixing the flow with their porous structures.

With the use of nanofluid on the empty surface, a 6.9% improvement in heat transfer was achieved compared to the base fluid. By passing the base fluid through 10 PPI and 40 PPI PHS, an improvement of 31.7% and 27.9% was obtained in the heat transfer relative to the empty surface, respectively. In the case of passing nanofluid, the amount of improvement obtained for both PHSs was determined as 52.3% and 62.7%, respectively.

The variation of the Nusselt number with respect to the Reynolds number as a result of using 10 PPI and 40 PPI PHS with nanofluid is given in Figure 9, together with different studies in the literature. As in the other studies, the Nusselt number increased with the increase in the Reynolds number with the use of nanofluids. In addition, it was seen that the Nusselt numbers obtained as a result of using nanofluid in both PHSs were of the same magnitude as the studies mentioned. However, the results obtained from the studies were different due to the use of PHS with a different foam structure, as well as the geometry, design and measurement parameters of the test region.

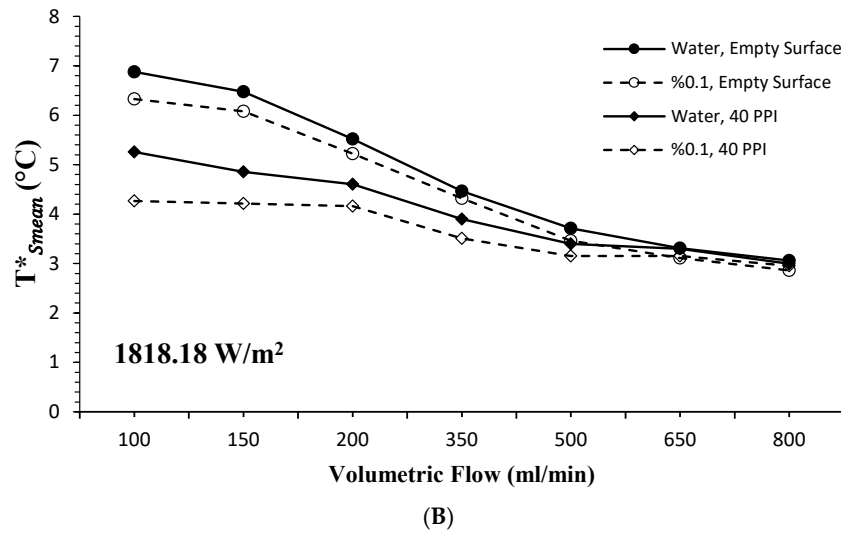
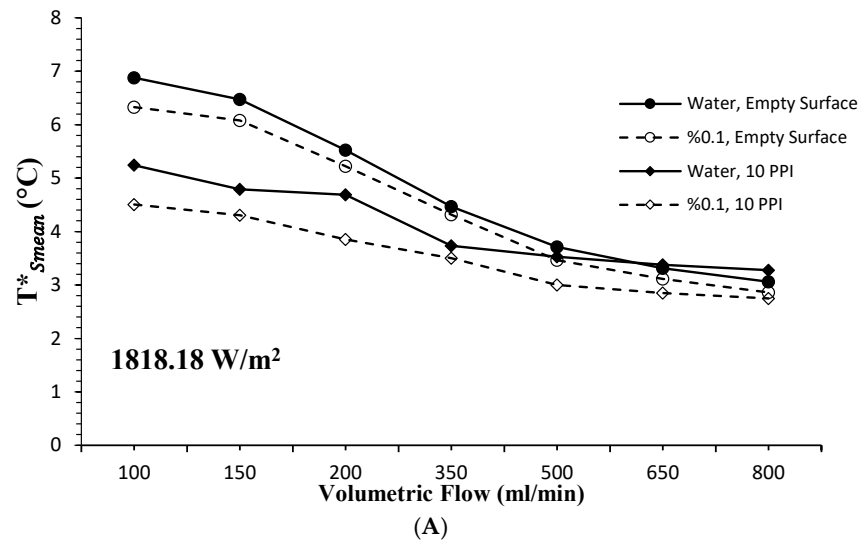


Figure 6. Mean surface temperatures versus volumetric flow rates with different PHSs (A) 10 PPI, (B) 40 PPI.

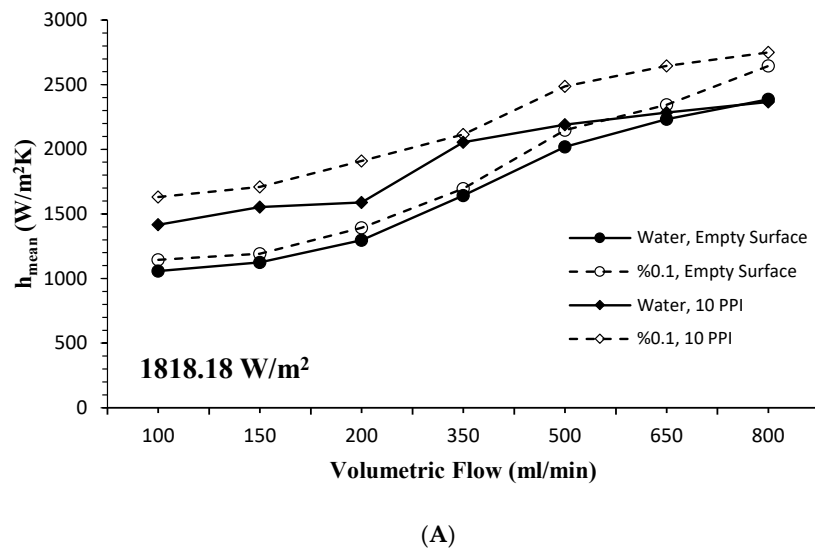
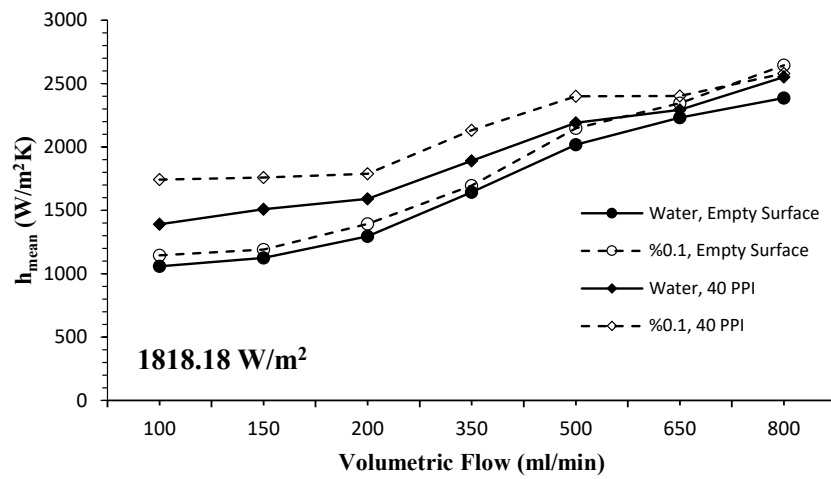
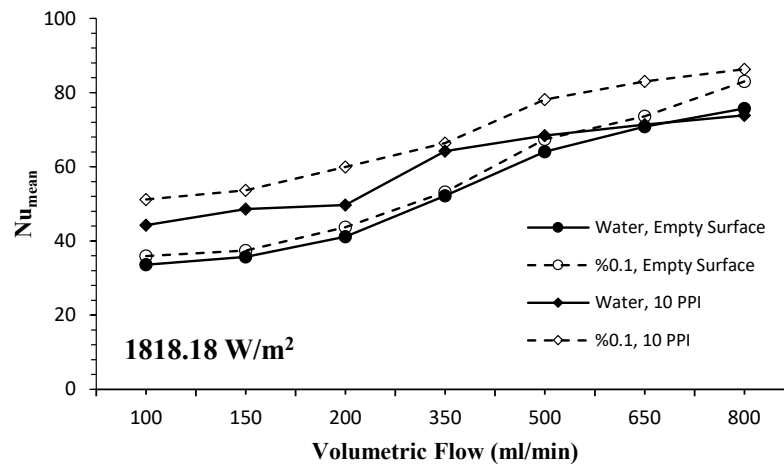


Figure 7. Cont.

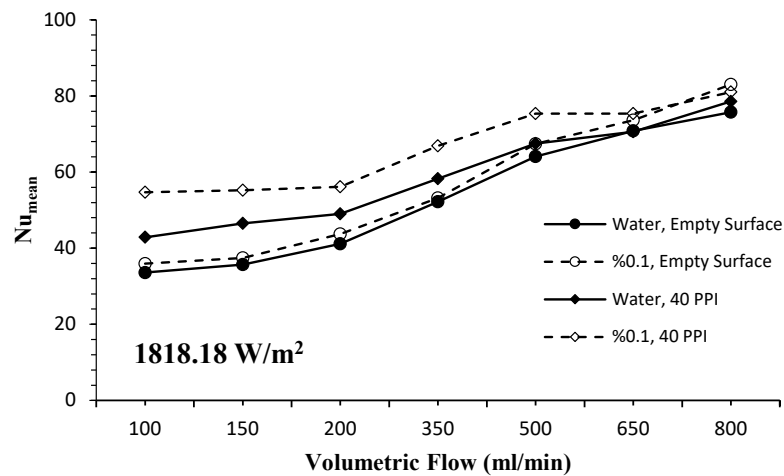


(B)

Figure 7. Variation of mean convective heat transfer coefficient with volume flow rate at 1818.18 W/m² (A) 10 PPI; (B) 40 PPI.



(A)



(B)

Figure 8. Variation of mean Nusselt number against volumetric flow rate as a result of using PHSs with nanofluid (A) 10 PPI; (B) 40 PPI.

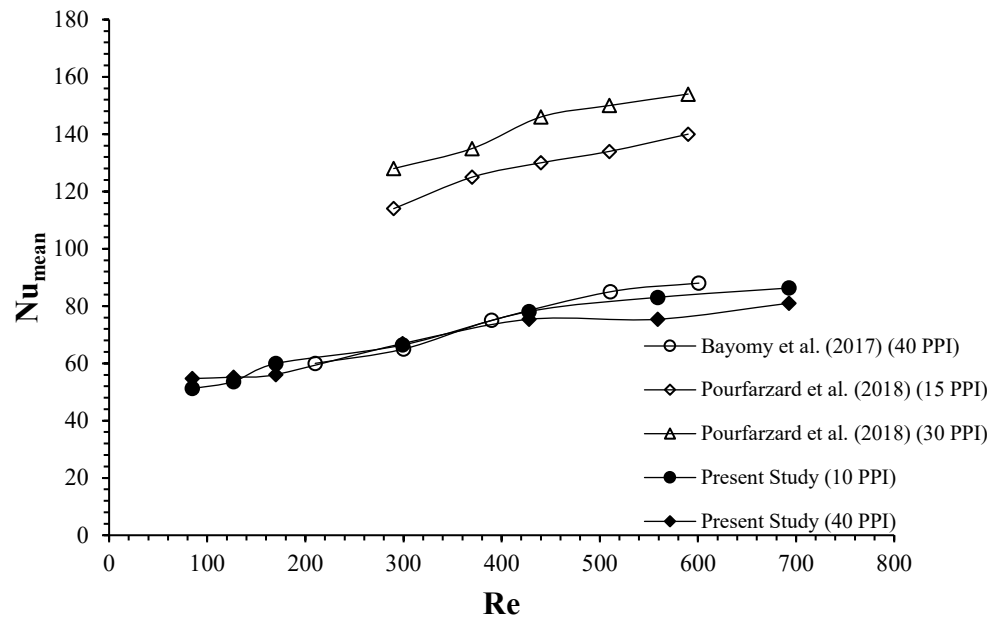


Figure 9. Variation of mean Nusselt number against Reynolds number in various studies Pourfarzard et al. [2], Bayomy et al. [4].

In the case of using 10 PPI and 40 PPI PHS with the nanofluid, the change in thermal resistance according to the volumetric flow were given in Figure 10A,B. A significant reduction in thermal resistance occurred at 10 PPI and 40 PPI PHS for both the base fluid and the nanofluid compared to the empty surface. Thermal resistance is a measure of a system’s ability to remove heat, and it varies inversely with heat transfer. A 6.33% decrease in thermal resistance was observed with the use of the nanofluid on the empty surface compared to the base fluid. With the use of 10 PPI and 40 PPI PHSs, a decrease of 16.9% for the base fluid and 23.48% for the nanofluid was determined.

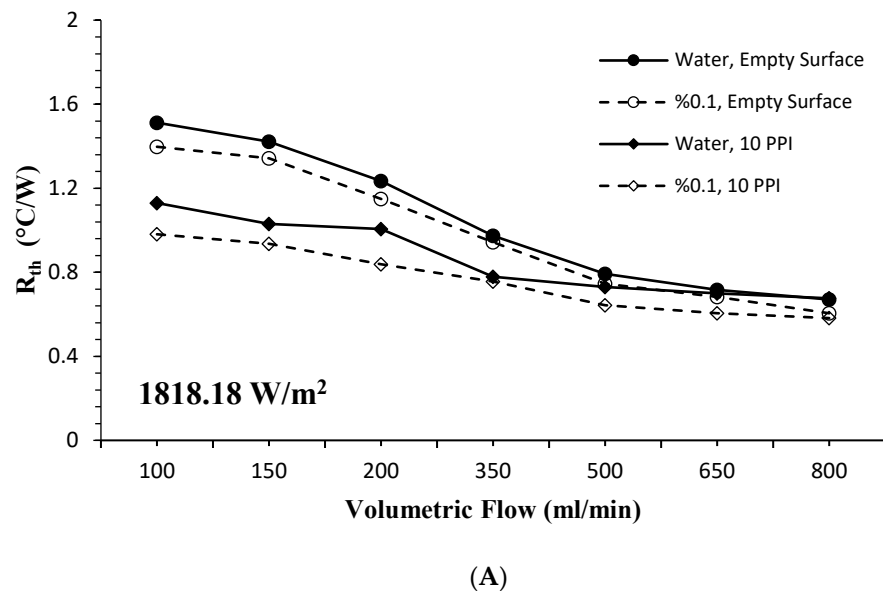


Figure 10. Cont.

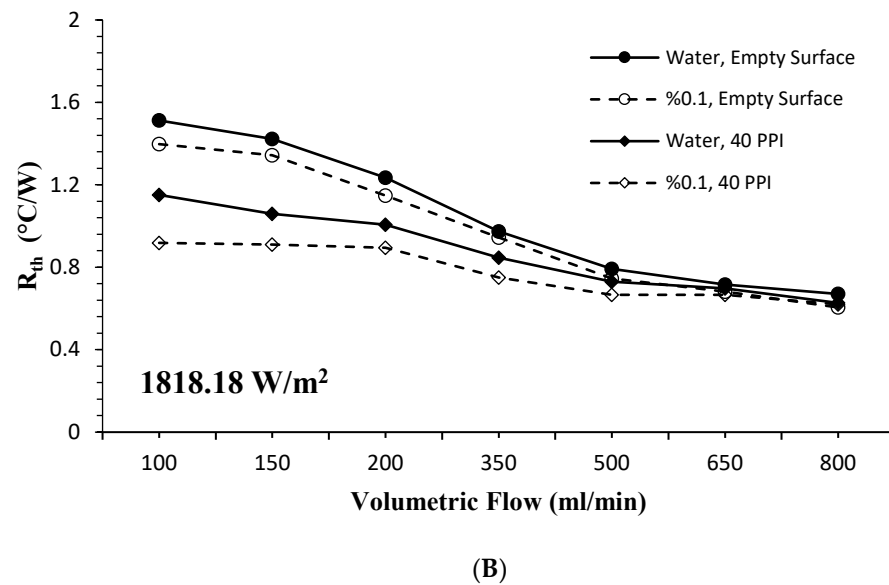


Figure 10. At 1818.18 W/m² constant heat flux, thermal performance variation with volume flow rate (A) 10 PPI; (B) 40 PPI.

The thermal performance of the nanofluid used for the empty surface at a heat flux of 454.54 W/m² compared to the base fluid is given in Figure 11. As seen in the figure, the thermal performance increased with the use of the nanofluid compared to the base fluid. In addition, the thermal performance value of the nanofluid increased with increasing volumetric flow. With the increase in volumetric flow, slight fluctuations in thermal performance occurred at certain values. These fluctuations in thermal performance values were due to the inability of the nanofluid to find sufficient contact time with the surface due to the increase in volumetric flow. Similar results were seen in the study of Khaleduzzaman et al. [46] examining the use of nanofluids in the cooling of electronic systems.

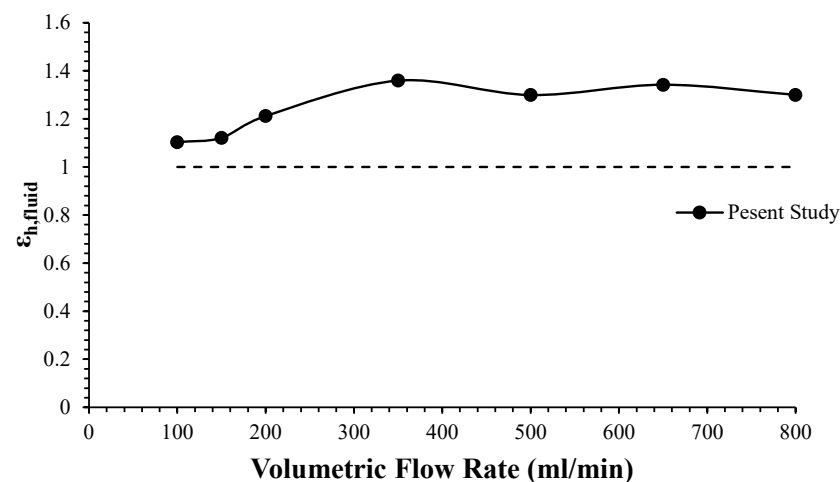


Figure 11. In empty channel, thermal performance of nanofluid according to volumetric flow.

The variation in pumping power according to the volumetric flow rate as a result of the use of the PHS and nanofluid is given in Figure 12. In all cases, there was no rapid increase in the pumping power up to 200 mL/min volumetric flow, while a significant increase in pumping power was observed at higher values of volumetric flow. It was seen that the pumping power required for the nanofluid was higher at the empty surface when compared to the base fluid, and it was also determined that this difference, which was observed with the use of PHSs, increased even more. The highest pumping power was obtained especially when the nanofluid and 40 PPI PHS were used together.

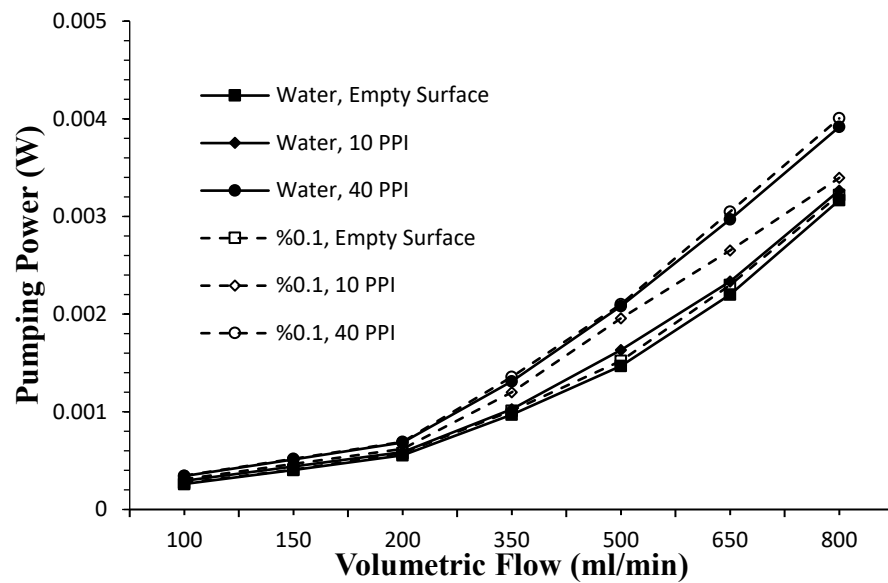


Figure 12. Pumping power for nanofluid and water for different volumetric flow rates.

The comparison of the improvement in heat transfer with the use of the nanofluid and PHS with the increase in pressure drop was made with the thermal performance value given in Equation (14). Accordingly, in the case of using the nanofluid and PHS in the test region, the variation of thermal performance with respect to the volumetric flow rate is given in Figure 13. It was observed that the thermal performance values obtained by using both 10 PPI PHS and 40 PPI PHS approach each other with increasing volumetric flow. The highest performance index was obtained with the use of 10 PPI metal PHS and nanofluids. The increase in pressure drop with the use of 40 PPI PHS and the nanofluid was more effective than the increase in the amount of heat transfer.

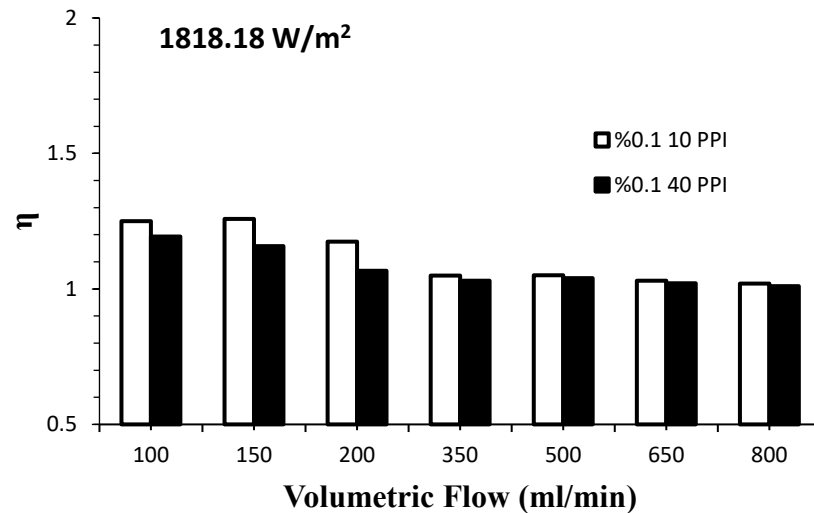


Figure 13. Thermal performance efficiency of 10 PPI and 40 PPI PHSs with nanofluid.

4. Conclusions

In the experimental study, the effect of the use of nanofluids and PHS on the thermal and pressure performance of the cooling of electronic systems was investigated. The $Al_2O_3-H_2O$ nanofluid with a concentration of 0.1% by mass was used as the refrigerant. The experimental study was conducted for a constant heat flux of $454.54 W/m^2$ and $1818.18 W/m^2$ and volumetric flow rates of 100 mL/min to 800 mL/min. The results obtained from 10 PPI and 40 PPI PHSs using both the base fluid and the nanofluid were compared with the empty surface.

- In the cooling of electronic systems, a significant increase in heat transfer compared to the empty surface was observed with the use of PHS for both the base fluid and the 0.1% mass concentration nanofluid.
- With the increase in the volumetric flow rate, the surface temperature was decreased due to the increased heat transfer. While the difference between the results obtained in heat transfer for all surfaces and both fluids was more pronounced at low volumetric flow rates, these differences gradually decreased at high volumetric flow rates.
- By using the Al₂O₃-H₂O nanofluid at a concentration of 0.1% by mass on the empty surface, the maximum improvement in heat transfer was determined as 6.9% compared to the base fluid.
- By using 10 PPI and 40 PPI PHS together with the base fluid, the highest improvement in the mean heat transfer coefficient was determined as 31.7% and 27.9%, respectively. With the use of 10 PPI and 40 PPI PHS together with the nanofluid, the highest improvement in the mean heat transfer coefficient was determined as 52.3% and 62.7%, respectively.
- With the use of nanofluid on the empty surface, the highest thermal performance value compared to the base fluid was determined as 1.36.
- With the use of nanofluid and 10 PPI and 40 PPI PHSs together, the highest values of thermal performance index values were determined as 1.258 and 1.193, respectively, compared to the blank surface.

These results suggest several guidelines for the thermal design of electronic systems. They recommend the use of the Al₂O₃-H₂O nanofluid with a concentration of 0.1% by mass in systems with low power dissipation and the use of both 10 PPI PHS and nanofluids in systems with high power dissipation. Accordingly, it is thought that the combined use of the investigated nanofluid and PHS may be more advantageous than fan systems in cooling the CPUs that experience the worst heating problems.

Author Contributions: Experimental setup, O.O. and A.D.; calibration, O.O. and A.D.; measurements, O.O.; formal analysis, O.O. and A.D., investigation, O.O., A.D. and M.A.; resources, O.O., A.D. and M.A.; data evaluation, O.O., A.D. and M.A.; Nanofluid preparation, M.A.; thermophysical property measurement, M.A. and O.O.; writing—original draft preparation, O.O., A.D. and M.A.; writing—review and editing, O.O., A.D. and M.A.; project administration, O.O. and A.D.; funding acquisition, O.O. All authors have read and agreed to the published version of the manuscript.

Funding: The financial support of this study by the research fund of Akdeniz University under Grant no: FBA-2019-4985 is gratefully acknowledged.

Data Availability Statement: The data presented in this study are available on request from the corresponding author.

Conflicts of Interest: The authors declare no conflict of interest.

Abbreviations

Symbols

A_c	Channel cross-sectional area [m ²]
A_s	Water block surface area [m ²]
C_p	Specific heat [J/kgK]
D_h	Hydraulic diameter [m]
h	Convective heat transfer coefficient [W/m ² K]
k	Thermal conductivity [W/mK]
k_f	Fluid conductive heat transfer coefficient [W/mK]
Nu	Average Nusselt Number [-]
P_p	Pumping power [W]
$\dot{Q}_{Cond.}$	Conduction heat transfer rate [W]
$\dot{Q}_{Conv.}$	Convection heat transfer rate [W]
\dot{Q}_{Heater}	Heat transfer rate from heater [W]
$q_{conv.}$	Convection heat flux [W/m ²]

P	Perimeter [m]
R	Electrical resistance [Ohm]
R_{th}	Thermal resistance [$^{\circ}\text{C}/\text{W}$]
T_i	Fluid inlet temperature [$^{\circ}\text{C}$]
T_{Smean}^*	Mean surface temperature [$^{\circ}\text{C}$]
V	Voltage [V]
ΔT	Temperature difference [$^{\circ}\text{C}$]
Δx	Thickness [m]
w_f	Uncertainty [-]
ε_h	Thermal performance of nanofluid [-]
η	Performance index [-]
ρ	Density (g/cm^3)
ν	Viscosity [m^2/s]
φ	Volumetric concentration [-]
ω	Mass fraction [-]
Subscripts	
bf	Base fluid
nf	Nanofluid
p	Nanoparticle
s	Surface
f	Fluid
Abbreviations	
PHS	Porous Heat Sink
PPI	Pores Per Inch

References

- Choi, S.U.S.; Eastman, J.A. Enhancing thermal conductivity of fluids with nanoparticles. In Proceedings of the ASME International Mechanical Engineering Congress & Exposition, San Francisco, CA, USA, 12–17 November 1995.
- Pourfarzad, E.; Ghadiri, K.; Behrangzade, A.; Ashjaee, M. Experimental Investigation of Heat Transfer and Pressure Drop of Alumina–Water Nano-Fluid in a Porous Miniature Heat Sink. *Exp. Heat Transfer*. **2018**, *31*, 495–512. [[CrossRef](#)]
- Bayomy, A.M.; Saghir, Z.; Yousefi, T. Electronic Cooling Using Water Flow in Aluminum Metal Foam Heat Sink: Experimental and Numerical Approach. *Int. J. Therm. Sci.* **2016**, *109*, 182–200. [[CrossRef](#)]
- Bayomy, A.M.; Saghir, Z. Experimental Study of Using $\gamma\text{-Al}_2\text{O}_3$ –Water Nanofluid Flow Through Aluminum Foam Heat Sink: Comparison with Numerical Approach. *Int. J. Heat Mass Transf.* **2017**, *107*, 181–203. [[CrossRef](#)]
- Bayomy, A.M.; Saghir, Z. Thermal Performance of Finned Aluminum Heat Sink Filled with ERG Aluminum Foam: Experimental and Numerical Approach. *Int. J. Energy Res.* **2020**, *44*, 4411–4425. [[CrossRef](#)]
- Bayomy, A.M.; Saghir, M.Z. Experimental and Numerical Study of the Heat Transfer Characteristics of Aluminium Metal Foam (with/without channels) Subjected to Steady Water Flow. *Pertanika J. Sci. Tech.* **2017**, *25*, 221–246.
- Qi, C.; Chen, T.; Tu, J.; Yan, Y. Effects of Metal Foam on Exergy and Entropy of Nanofluids in a Heat Sink Applied for Thermal Management of Electronic Components. *Int. J. Energy Res.* **2020**, *44*, 10628–10651. [[CrossRef](#)]
- Boomsma, K.; Poulikakos, D.; Zwicky, F. Metal Foams as Compact High Performance Heat Exchangers. *Mech. Mater.* **2003**, *35*, 1161–1176. [[CrossRef](#)]
- Saghir, M.Z.; Welsford, C. Forced Convection in Porous Media Using Al_2O_3 and TiO_2 Nanofluids in Differing Base Fluids. *Energies* **2020**, *13*, 2665. [[CrossRef](#)]
- Delise, C.S.; Westford, C.A.; Saghir, M.Z. Forced Convection Study with Microporous Channels and Nanofluid: Experimental and Numerical. *J. Therm. Anal. Calorim.* **2020**, *140*, 1205–1214. [[CrossRef](#)]
- Ameri, M.; Amani, M.; Amani, P. Thermal Performance of Nanofluids in Metal Foam Tube: Thermal Dispersion Model Incorporating Heterogeneous Distribution of Nanoparticles. *Adv. Powder Technol.* **2017**, *28*, 2747–2755. [[CrossRef](#)]
- Nazari, M.; Ashouri, M.; Kayhani, M.H.; Tamayol, A. Experimental Study of Convective Heat Transfer of a Nanofluid Through a Pipe Filled with Metal Foam. *Int. J. Therm. Sci.* **2015**, *88*, 33–39. [[CrossRef](#)]
- Rabbani, P.; Hamzeshpour, A.; Ashjaee, M.; Najafi, M.; Houshfar, E. Experimental Investigation on Heat Transfer of MgO Nanofluid in Tubes Partially Filled with Metal Foam. *Powder Technol.* **2019**, *354*, 734–742. [[CrossRef](#)]
- Khoshvaght-Aliabadi, M.; Hormozi, F. Heat Transfer Enhancement by Using Copper–Water Nanofluid Flow Inside a Pin Channel. *Exp. Heat Transf.* **2015**, *28*, 446–463. [[CrossRef](#)]
- Miry, S.Z.; Roshani, M.; Hanafizadeh, P.; Ashjaee, M.; Amini, F. Heat Transfer and Hydrodynamic Performance Analysis of a Miniature Tangential Heat Sink Using $\text{Al}_2\text{O}_3\text{-H}_2\text{O}$ and $\text{TiO}_2\text{-H}_2\text{O}$ Nanofluids. *Exp. Heat Transf.* **2016**, *29*, 535–560. [[CrossRef](#)]
- Dogan, A.; Ozbalci, O.; Atmaca, I. Experimental investigation of natural convection from porous blocks in a cavity. *J. Porous Media* **2016**, *19*, 1023–1032. [[CrossRef](#)]

17. Ozbalci, O.; Dogan, A. Forced convection heat transfer from porous heat sinks placed in partially open cavity: Some case studies. *Exp. Heat Transf.* **2018**, *31*, 183–193. [[CrossRef](#)]
18. Dogan, A.; Ozbalci, O. Experimental investigation of free convection from foam heat sinks in an inclined rectangular channel. *Cumhuriyet Sci. J.* **2018**, *39*, 756–765. [[CrossRef](#)]
19. Abadi, G.B.; Kim, K.C. Experimental heat transfer and pressure in a metal foam-filled tube heat exchanger. *Exp. Therm. Fluid Sci.* **2017**, *82*, 42–49. [[CrossRef](#)]
20. Bhattacharya, A.; Mahajan, R.L. Finned metal foam heat sinks for electronic cooling in forced convection. *J. Electron. Packag.* **2002**, *124*, 155–163. [[CrossRef](#)]
21. Li, Y.; Gong, L.; Xu, M.; Joshi, Y. Enhancing the performance of aluminum foam heat sinks through integrated pin fins. *Int. J. Heat Mass Transfer* **2020**, *151*, 119376. [[CrossRef](#)]
22. Li, Y.; Gong, L.; Ding, B.; Xu, M.; Joshi, Y. Thermal management of power electronics with liquid cooled metal foam heat sink. *Int. J. Therm. Sci.* **2021**, *163*, 106796. [[CrossRef](#)]
23. Nguyen, C.T.; Roy, G.; Gauthier, C.; Galanis, N. Heat transfer enhancement by using Al₂O₃-water nanofluid for an electronic liquid cooling system. *Appl. Therm. Eng.* **2007**, *27*, 1501–1506. [[CrossRef](#)]
24. Selvakumar, P.; Suresh, S. Convective performance of CuO/water nanofluid in an electronic heat sink. *Exp. Therm. Fluid Sci.* **2012**, *40*, 57–63. [[CrossRef](#)]
25. Rafati, M.; Hamidi, A.A.; Niaser, M.S. Application of nanofluids in computer cooling systems (heat transfer performance of nanofluids). *Appl. Therm. Eng.* **2012**, *45*, 9–14. [[CrossRef](#)]
26. Nazari, M.; Karami, M.; Ashouri, M. Comparing the thermal performance of water, ethylene glycol, alumina and CNT nanofluids in CPU cooling: Experimental study. *Exp. Therm. Fluid Sci.* **2014**, *57*, 371–377. [[CrossRef](#)]
27. Qi, C.; Hu, J.; Liu, M.; Guo, L.; Rao, Z. Experimental Study on Thermo-Hydraulic Performances of Cpu Cooled by Nanofluids. *Energy Convers. Manag.* **2017**, *153*, 557–565. [[CrossRef](#)]
28. Ho, C.J.; Liao, J.C.; Li, C.H.; Yan, W.M.; Amani, M. Experimental study of cooling characteristics of water-based alumina nanofluid in a minichannel heat sink. *Case Stud. Therm. Eng.* **2019**, *14*, 100418. [[CrossRef](#)]
29. Zhao, N.; Guo, L.; Qi, C.; Chen, T.; Cui, X. Experimental study on thermo-hydraulic performance of nanofluids in CPU heat sink with rectangular grooves and cylindrical bugles based on exergy efficiency. *Energy Convers. Manag.* **2019**, *181*, 235–246. [[CrossRef](#)]
30. Bahiraie, M.; Mazaheri, N.; Daneshyar, M.R. Employing elliptical pin-fins and nanofluid within a heat sink for cooling of electronic chips regarding energy efficiency perspective. *Appl. Therm. Eng.* **2021**, *183*, 116159. [[CrossRef](#)]
31. Alfaryjat, A.A.; Miron, L.; Pop, H.; Apostol, V.; Stefanescu, M.F.; Dobrovicescu, A. Experimental Investigation of Thermal and Pressure Performance in Computer Cooling Systems Using Different Types of Nanofluids. *Nanomaterials* **2019**, *9*, 1231. [[CrossRef](#)]
32. Ali, H.M.; Arshad, W. Thermal performance investigation of staggered and inline pin fin heat sinks using water based rutile and anatase TiO₂ nanofluids. *Energy Convers. Manag.* **2015**, *106*, 793–803. [[CrossRef](#)]
33. Ali, H.M.; Arshad, W. Effect of channel angle of pin-fin heat sink on heat transfer performance using water based graphene nanoplatelets nanofluids. *Int. J. Heat Mass Transf.* **2017**, *106*, 465–472. [[CrossRef](#)]
34. Hassani, S.M.; Aliabadi, M.K.; Mazloumi, S.H. Influence of chevron fin interruption on thermo-fluidic transport characteristics of nanofluid-cooled electronic heat sink. *Chem. Eng. Sci.* **2018**, *191*, 436–447. [[CrossRef](#)]
35. Sajid, M.U.; Ali, H.M.; Sufyan, A.; Rashid, D.; Zahid, S.U.; Rehman, W.U. Experimental investigation of TiO₂-water nanofluid flow and heat transfer inside wavy mini-channel heat sinks. *J. Therm. Anal. Calorim.* **2019**, *137*, 1279–1294. [[CrossRef](#)]
36. Sajid, M.U.; Ali, H.M.; Bicer, Y. Exergetic performance assessment of magnesium oxide-water nanofluid in corrugated minichannel heat sinks: An experimental study. *Int. J. Energy Res.* **2020**, *46*, 9985–10001. [[CrossRef](#)]
37. Hashemzadeh, S.; Hormozi, F. An experimental study on hydraulic and thermal performances of hybrid nanofluids in minichannel. *J. Therm. Anal. Calorim.* **2020**, *140*, 891–903. [[CrossRef](#)]
38. Hwang, K.S.; Jang, S.P.; Choi, S.U.S. Flow and convective heat transfer characteristics of water-based Al₂O₃ nanofluids in fully developed laminar flow regime. *Int. J. Heat Mass Transf.* **2009**, *52*, 193–199. [[CrossRef](#)]
39. Kim, S.; Tserengombo, B.; Choi, S.H.; Noh, J.; Huh, S.; Choi, B.; Chung, H.; Kim, J.; Jeong, H. Experimental investigation of heat transfer coefficient with Al₂O₃ nanofluid in small diameter tubes. *Appl. Therm. Eng.* **2019**, *146*, 346–355. [[CrossRef](#)]
40. Aliabadi, M.K.; Sartipzadeh, O.; Pazdar, S.; Sahamiyan, M. Experimental and parametric studies on a miniature heat sink with offset-strip pins and Al₂O₃/water nanofluids. *Appl. Therm. Eng.* **2017**, *111*, 1342–1352. [[CrossRef](#)]
41. Anoop, K.B.; Sundararajan, T.; Das, S.K. Effect of particle size on the convective heat transfer in nanofluid in the developing region. *Int. J. Heat Mass Transf.* **2009**, *52*, 2189–2195. [[CrossRef](#)]
42. Duangthongsuk, W.; Wongwises, S. A comparison of the heat transfer performance and pressure drop of nanofluid-cooled heat sinks with different miniature pin fin configurations. *Exp. Therm. Fluid Sci.* **2015**, *69*, 111–118. [[CrossRef](#)]
43. Ghasemi, S.E.; Ranjbar, A.A.; Hosseini, M.J. Experimental evaluation of cooling performance of circular heat sinks for heat dissipation from electronic chips using nanofluid. *Mech. Res. Commun.* **2017**, *84*, 85–89. [[CrossRef](#)]
44. Nadeem, S.; Qadeer, S.; Akhtar, S.; Almutairi, S.; Wang, F.Z. Mathematical model of convective heat transfer for peristaltic flow of Rabinowitsch fluid in a wavy rectangular duct with entropy generation. *Phys. Scr.* **2022**, *97*, 88. [[CrossRef](#)]
45. Nadeem, S.; Qadeer, S.; Akhtar, S.; El Shafey, A.M.; Issakhov, A. Eigenfunction expansion method for peristaltic flow of hybrid nanofluid flow having single-walled carbon nanotube and multi-walled carbon nanotube in a wavy rectangular duct. *Sci. Prog. UK* **2021**, *104*, 292. [[CrossRef](#)]

46. Ghazwani, H.A.; Akhtar, S.; Almutairi, S.; Saleem, A.; Nadeem, S.; Mahmoud, O. Insightful facts on peristalsis flow of water conveying multi-walled carbon nanoparticles through elliptical ducts with ciliated walls. *Front. Phys.* **2022**, *10*, 551. [[CrossRef](#)]
47. Nadeem, S.; Akhtar, S.; Alharbi, F.M.; Saleem, S.; Issakhov, A. Analysis of heat and mass transfer on the peristaltic flow in a duct with sinusoidal walls: Exact solutions of coupled PDEs. *Alex. Eng. J.* **2022**, *61*, 4107–4117. [[CrossRef](#)]
48. Aerioxide. Aerioxide, Alu-130. Evonik Industries. 2013. Available online: <https://glennncorp.com/wp-content/uploads/2013/12/AEROXIDE-Alu-130.pdf> (accessed on 10 July 2022).
49. Calvin, J.J.; Asplund, M.; Zhang, Y.; Huang, B.; Woodfield, B.F. Heat Capacity and Thermodynamic Functions of γ -Al₂O₃. *J. Chem. Thermodyn.* **2017**, *112*, 77–85. [[CrossRef](#)]
50. Prakash, A.; Satsangi, S.; Mittal, S.; Nigam, B.; Mahto, P.K.; Swain, B.P. Investigation on Al₂O₃ Nanoparticles for Nanofluid Applications- A Review. *IOP Conf. Ser. Mater. Sci. Eng.* **2018**, *377*, 012175. [[CrossRef](#)]
51. Khaleduzzaman, S.; Mahbubul, I.; Sohel, M.; Saidur, R.; Selvaraj, J.; Ward, T.; Niza, M. Experimental Analysis of Energy and Friction Factor for Titanium Dioxide Nanofluid in a Water Block Heat Sink. *Int. J. Heat Mass Transf.* **2017**, *115*, 77–85. [[CrossRef](#)]
52. Holman, J.P. Analysis of Experimental Data. In *Experimental Methods for Engineers*, 6th ed.; McGraw-Hill Inc.: New York, NY, USA, 1994; pp. 49–56.